PERGAMON

International Journal of Solids and Structures 37 (2000) 577–598

INTERNATIONAL JOURNAL OF SOLIDS and STRUCTURES

www.elsevier.com/locate/ijsolstr

Fully plastic crack-tip fields for CCP and DECP specimens under tension in non-hardening materials

X.K. Zhu, Y.J. Chao*

Department of Mechanical Engineering, University of South Carolina, Columbia SC 29208, USA

Received 28 March 1998

Abstract

Detailed finite element analyses are performed for center cracked plate (CCP) and double edge cracked plate (DECP) in non-hardening materials under plane strain conditions. The objective is to systematically investigate the effects of deformation level, loading type, crack depth and specimen dimension on crack-tip fields and constraints of these two specimens. Special attention is placed on (a) under what conditions the slip-line fields can be present near the crack tip, and (b) determining what deformation mechanism makes the crack-tip fields significantly different in the two specimens at fully plastic state.

The results reveal that (a) at load levels much smaller than the limit load (i.e., small-scale yielding) the crack-tip fields are close to the Prandtl field for both specimens, (b) the effects of crack depth a/W on the crack-tip field is not remarkable for CCP, but significant for DECP at the limit load, (c) as $L/W \geq 2.4$ for CCP and $L/W \geq 2$ for DECP, the crack-tip fields are independent of the specimen length L/W, (d) at the limit load, the crack face is under compression for all CCP, and (e) a compression (tensile) zone exists at the crack face of shallow (deep) cracked DECP. Moreover, it is found that there exist tensile and compressive stresses along the vertical centerline of specimen for both CCP and DECP which result in a bending moment M_{VL}. The difference between M_{VL} and the moment generated by the applied far-field loads makes the crack opening stress *non-uniform* along the remaining ligament. Recall that the slip-line fields for both the CCP and DECP have *uniform* opening stress along the ligament. At the limit load, therefore, the numerical crack-tip stress fields can only approach to, but *cannot* attain to, the slip-line fields for both CCP and DECP specimens.

In addition, through comparison of the different limit loads given for DECP specimens, the present results indicate that the limit load formula given by Kumar *et al.* (EPRI, 1981) is valid only for $0.4 \leq a/W \leq 0.7$, whereas the formula of Ewing and Hill (1967) can be used for any crack depth.

Keywords: Finite element analysis; CCP; DECP; Plane strain; Crack-tip field; Slip-line field; Full plasticity

* Corresponding author. Fax: +001-803-7777-0106.
E-mail address: chao@sc.edu (Y.J. Chao)

0020-7683/00/$ - see front matter
PII: S0020-7683(99)00024-4

1. Introduction

Characterization of crack-tip stress and strain fields is fundamental to the interpretation of fracture of solids. Furthermore, the crack-tip constraint affects the fracture toughness of test specimens; thus is important for integrity assessment of engineering structures. For power-law hardening materials, Hancock et al. (1993), Shih et al. (1993) and Chao et al. (1994) have quantified the constraint of crack-tip fields by using J-T, J-Q and J-A_2 parameters, respectively, for cracked specimens with different geometry and loading configurations. Chao and Zhu (1998) summarized the results of crack-tip fields in hardening materials and investigated the dominance of J-A_2 characterization (Yang et al., 1993) and size requirements of specimens for a valid J-A_2 two-parameter fracture testing. For elastic-perfectly plastic or non-hardening materials, Lee and Parks (1993) carried out fully plastic numerical analyses of single edge cracked specimen subjected to different combined tension and bending for a deep crack of $a/W = 0.5$. Kim et al. (1996) performed detailed finite element analyses to study the effect of crack depth on crack-tip constraint at full yielding for single edge cracked specimens under pure bending. More recently, Zhu and Chao (1999) characterized the constraint of crack-tip fields for several conventional specimens in non-hardening materials under the framework of the J-A_2 description.

At the state of complete yielding of a specimen, analyses based on perfect plasticity, such as the slip-line field and finite element analysis, could provide meaningful insights and reference values for low hardening structural materials, and possibly for moderate-hardening materials. McClintock (1971) showed that the stress and velocity slip-line fields around a notch or sharp crack tip are generally different for different specimens under fully plastic conditions. In other words, the slip-line fields depend on the specimen geometry, crack depth and loading configuration. Miller (1988) and Wu et al. (1990) summarized the limit loads and the slip-line fields for several conventional fracture-testing specimens including both deep and shallow cracks. Among commonly used test specimens, CCP and DECP are the representatives of the low and high constraint specimens, respectively, with significantly different limit loads and slip-line fields from each other. Thus, one of the objectives of the current paper is to study the deformation mechanism that induces the difference in the mechanics behavior of CCP and DECP specimens, which cannot be given by slip-line fields.

The fracture toughness of a material is typically obtained by testing either compact tension (CT) or single edge notched bending (SENB) specimens. However, there is considerable interest in use of other specimens such as CCP and DECP (Lei and Neale, 1997). The CCP and DECP specimens enable the effect of constraint at other levels and offer the potential to reduce conservative estimates from SENB or CT specimens. McClintock (1971) gave the slip-line fields of CCP and DECP with deep cracks. Ewing and Hill (1967) presented the slip-line fields of DECP for both deep and shallow cracks. Goldman and Hutchinson (1975) analyzed fully plastic crack problems in a center-cracked strip. Kumar et al. (1981) presented limit load results of both CCP and DECP. Leevers and Radon (1982) studied the influence of geometry on the elastic T-stress in CCP. Lee and Liebowitz (1977), Jansson (1986) and O'Dowd et al. (1999) obtained finite element numerical values of J-integral for CCP in hardening materials under uniaxial and biaxial loading. Shaw and Huang (1990) showed that buckling can occur in a thin CCP under uniaxial tensile loads, whereas Quirk et al. (1966) and Quirk and Bevitt (1991) found that CCP geometry assures stable crack growth when other test specimen geometries exhibit unstable crack growth. Shih and German (1981), O'Dowd and Shih (1992), Chao and Zhu (1998) investigated CCP in power-law materials to determine J (or J-A_2) dominance zone and constraint levels. However, no complete investigation has yet been reported for the crack-tip fields (or constraints) and deformation mechanism of CCP and DECP with different crack depths, specimen lengths and loading types in non-hardening materials under various deformation levels.

In this paper, detailed finite element analyses (FEA) for CCP and DECP specimens subjected to

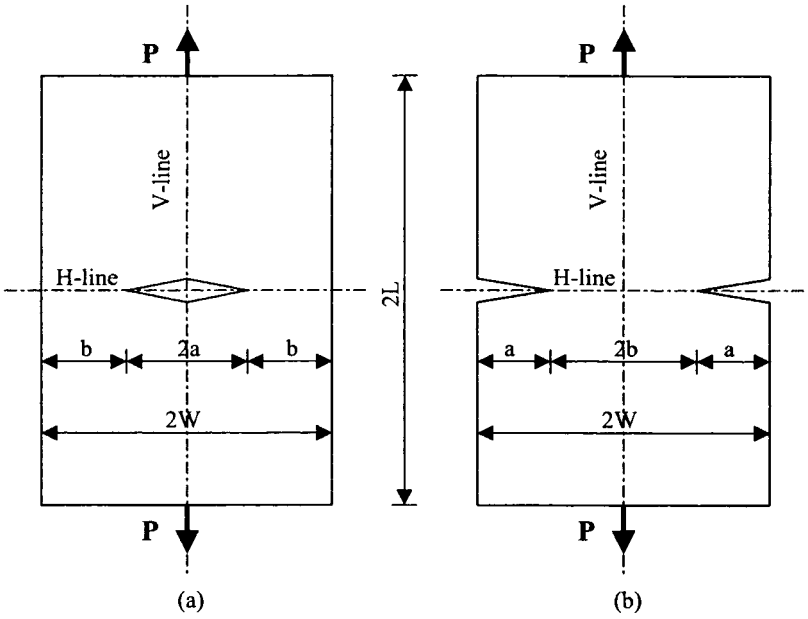

Fig. 1. Specimens and dimensions considered in this work (a) central cracked plate (CCP) and (b) double edge cracked plate (DECP).

remote tension are performed. Small deformation and plane strain conditions for non-hardening materials are considered. The objective is to systematically investigate the effects of deformation level, loading type, crack depth and specimen dimension on crack-tip fields and constraints of CCP and DECP. Special attention is focused on (a) under what conditions the slip-line fields can be attained near

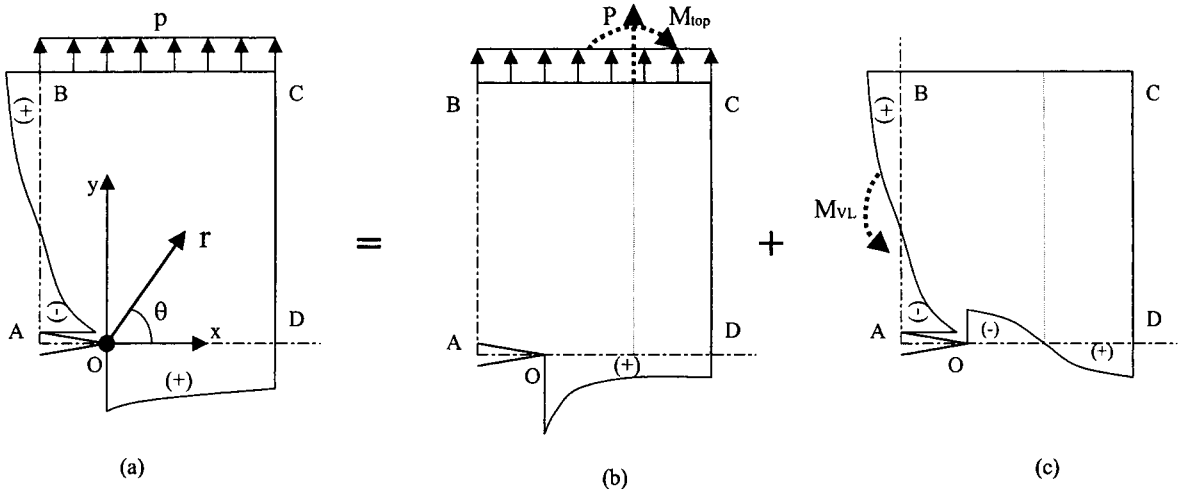

Fig. 2. Schematic stress distributions along the boundaries of one quadrant of a CCP specimen under uniformly distributed loads and the coordinate systems at the crack tip (p is uniformly distributed load, $P = pWB$ is concentrated force, M_{VL} and $M_{top} = paWB/2$ are moments. Positive sign denotes tensile stress and negative sign denotes compressive stress).

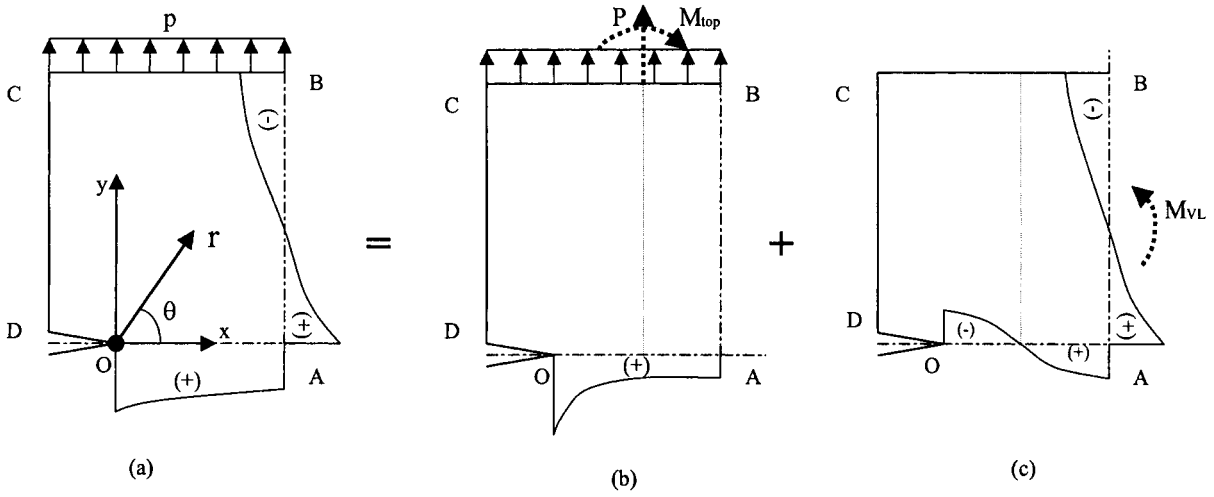

Fig. 3. Schematic stress distributions along the boundaries of one quadrant of a DECP specimen under uniformly distributed loads and the coordinate systems at the crack tip (p is uniformly distributed load, $P = pWB$ is concentrated force, M_{VL} and $M_{top} = paWB/2$ are moments. Positive sign denotes tensile stress and negative sign denotes compressive stress).

the crack tip and (b) determining what deformation mechanism makes the crack-tip fields significantly different for the two specimens at fully plastic yielding. In addition, several formulae for limit load of DECP specimens are compared and discussed. In the following, Section 2 introduces the specimen geometry and numerical model employed in the FEA. Section 3 and Section 4 present and discuss the FEA results of crack-tip stress fields and constraints for these specimens.

2. Geometry and finite element analysis model

Consider a CCP specimen and a DECP specimen subjected to remote tensile loading, as shown in Fig. 1(a) and (b), in which $2W$, $2L$, $2a$ and $2b$ are the plate width, plate length, crack depth and the length of uncracked ligament, respectively. Specimen thickness is denoted by B. It is assumed that in all cases the specimens are mounted in a vertical plane with vertically loading and a horizontal crack. The horizontal and vertical symmetric centerlines of the specimens are denoted by H-line and V-line, respectively. Due to symmetry, only one quadrant of the CCP or DECP is analyzed.

Fig. 2(a) shows schematically the stress distributions along the boundaries of one quadrant of a CCP specimen for a uniformly distributed applied load. The stress variations along the ligament OD could be approximately considered as the superposition of the stresses caused by the applied loads on the top edge BC, as shown in Fig. 2(b), and the stresses caused by the internal stresses on the V-line AB, as shown in Fig. 2(c). The crack opening stresses along OD is generally non-uniform because at the mid-ligament (i.e. the middle of ligament) the moment M_{top} generated by the applied load is not less than the bending moment M_{VL} resulted from the tensile and compressive stresses on the V-line, i.e. $M_{VL} \leq M_{top}$. Similarly, the stress distributions along the boundaries of one quadrant of a DECP specimen are schematically shown in Fig. 3(a) for the uniformly distributed applied load. The stress distributions along the ligament OA are not uniform and could be considered approximately as the superposition of two configurations, i.e. Fig. 3(b) and (c). In general, the relationship $M_{VL} \leq M_{top}$ also exists.

Note that if the applied loading is through rigid clamp on the ends, the stress distributions along all

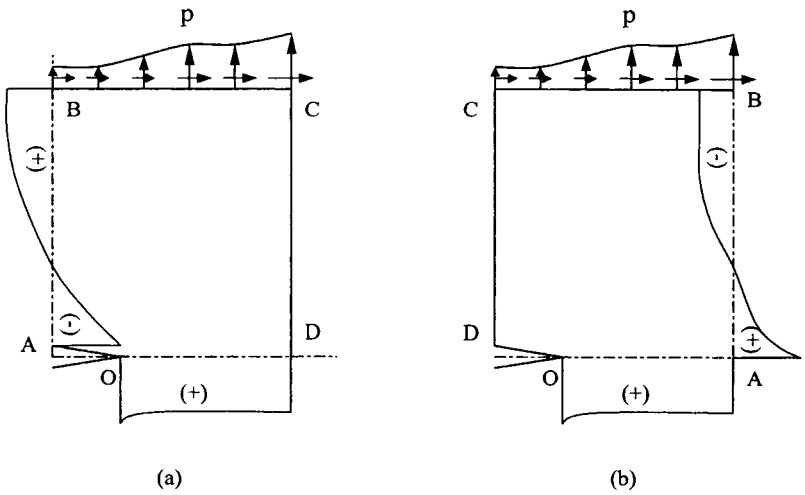

Fig. 4. Schematic stress distributions along the boundaries of one quadrant of (a) CCP and (b) DECP specimens under uniform rigid displacement. (Positive sign denotes tensile stress and negative sign denotes compressive stress).

boundaries of CCP and DECP can be shown qualitatively in Fig. 4. Due to the deformation constraint on the top edge *BC*, the applied stresses on *BC* would have both vertical and horizontal components and they are not uniform. Since the applied vertical stress is higher (lower) in the central region of DECP (CCP), the top moment M_{top} and consequently the moment difference $(M_{top} - M_{VL})$ could be less than that for uniformly distributed loads shown in Fig. 2 or Fig. 3. Therefore, the degree of non-uniformity of the stress distributions on the ligament for rigid displacements loading could be less than that for distributed loads. In the case of displacement loading, the stress distributions on the ligament could possibly approach the uniform state at the limit load.

Plane strain finite element analyses (FEA) were conducted to obtain detailed crack-tip stress fields for CCP and DECP specimens with deep and shallow cracks under remote tension. The deep crack specimens have $a/W = 0.5$ and 0.9 for CCP, $a/W = 0.9$ and 0.95 for DECP. The shallow crack

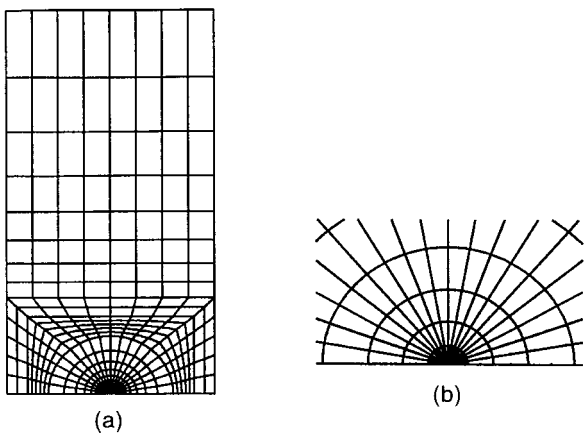

Fig. 5. Finite element mesh for the specimen analyzed which comprises of eight-node plane strain isoparametric elements. (a) The entire mesh with 604 elements and 1925 nodes, (b) the focused crack-tip mesh with eighteen side-collapsed elements.

specimens have $a/W = 0.1$ for CCP and $a/W = 0.5$ for DECP. Due to symmetry, only one quarter of both CCP and DECP, as shown in Fig. 2(a) and Fig. 3(a), was modeled. Appropriate symmetric boundary conditions were applied on the planes of symmetry. Loadings from very small to limit load were applied. The numerical models employed the small-strain formulations. The material was modeled as an isotropic elastic-plastic material obeying the non-hardening J_2 flow theory associated with the von Mises yield rule. In this work, the material is assumed to have the tensile yield strength $\sigma_0 = 445$ MPa and Young's modulus $E = 222.5$ GPa. Specimen half-width W is taken as 50 mm and specimen half-length $L = 3W$, unless specified otherwise.

The finite element mesh shown in Fig. 5 is used for both specimens. To avoid problems associated with incompressibility, eight-node plane strain, second order isoparametric elements with reduced integration (element type CPE8R from ABAQUS in version 5.6-1 (Hibbitt et al., 1997)) are employed in all FEA calculations. Eighteen eight-node elements degenerated into wedge shape comprise the upper half of the crack tip and twenty rings of elements are surrounding the crack tip. The innermost ring of the elements has one side collapsed onto the crack tip. All the nodes in the collapsed side can be separated after the loading is applied. The radial extent of the innermost ring element is about $1.34 \times 10^{-4}b$ (where b is the ligament length) for deep crack specimens and $1.34 \times 10^{-4}a$ (where a is the crack depth) for shallow cracked specimens. A typical finite element model has about 1925 nodes and 604 elements.

Two types of loading conditions are applied on the top edge of the FEA model: one is uniformly distributed applied load and the other is uniform rigid displacement. ABAQUS code uses a very stringent criterion to ensure convergence of strains and stresses in the J_2 flow theory of plasticity. In general, three to five iterations are required for convergence in each load step. Under small-scale yielding, speeds of convergence are the same for the two loading types. At large-scale yielding and at load levels approaching the limit load, however, there exists some difference in convergence speeds for the two loading types. FEA calculations in ABAQUS are easier to converge to the limit state for the case of rigid displacements than the applied loads. The magnitude of applied displacements can be made large enough to bring the specimens to their limit load state. The corresponding limit load can be determined from the nodal reactions on the top edge.

3. Fully plastic crack-tip fields for CCP specimen

In this section, we report our FEA results for CCP specimens and discuss the effects of deformation level or magnitude of applied load, loading type (uniformly distributed loads or uniform rigid displacements), crack depth (a/W) and specimen length (L/W) on the crack-tip stress field or constraint. Particular emphasis is placed on under what conditions the crack-tip stress field can reach the CCP slip-line field (McClintock, 1971) given by:

$$\sigma_{rr}(\theta) = \frac{2}{\sqrt{3}}\sigma_0(1 - \cos 2\theta)$$

$$\sigma_{\theta\theta}(\theta) = \frac{2}{\sqrt{3}}\sigma_0(1 + \cos 2\theta), \quad 0^\circ \le \theta \le 45^\circ \text{ and } 0 \le x \le b \tag{1}$$

$$\sigma_{r\theta}(\theta) = \frac{2}{\sqrt{3}}\sigma_0 \sin 2\theta$$

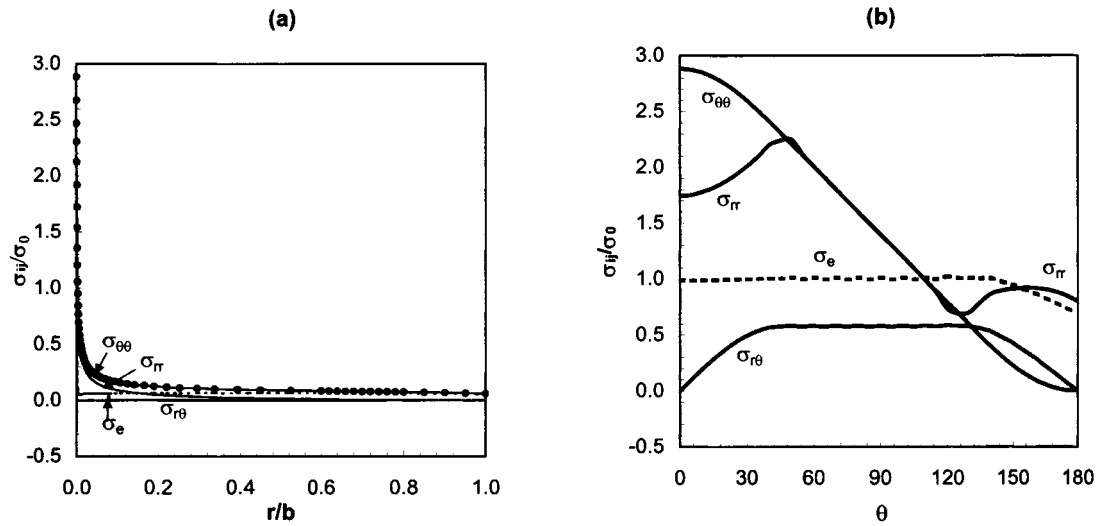

Fig. 6. Stress distributions of CCP specimen with $a/W = 0.5$ and $L/W = 3$ for uniformly distributed load $P = 0.1P_L$. (a) Radial distribution of stresses along the uncracked ligament, (b) angular distribution of stresses at $r = 0.0005b$.

Based on this slip-line field, the limit load (resultant) P_L of the CCP specimen is given by

$$P_L = \frac{4}{\sqrt{3}}(W - a)B\sigma_0 \tag{2}$$

In this section, unless specified otherwise, the dimensions of the CCP specimen are $a/W = 0.5$ and $L/W = 3$; loading type is the uniformly distributed load for small deformation levels and is the uniform

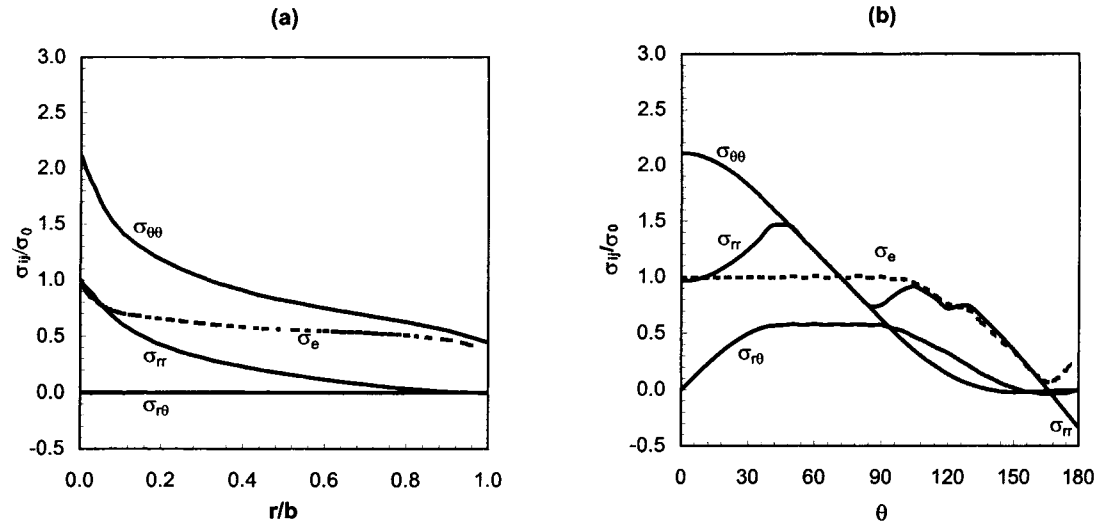

Fig. 7. Stress distributions of CCP specimen with $a/W = 0.5$ and $L/W = 3$ for uniformly distributed load $P = 0.8P_L$. (a) Radial distribution of stresses along the uncracked ligament, (b) angular distribution of stresses at $r = 0.05b$.

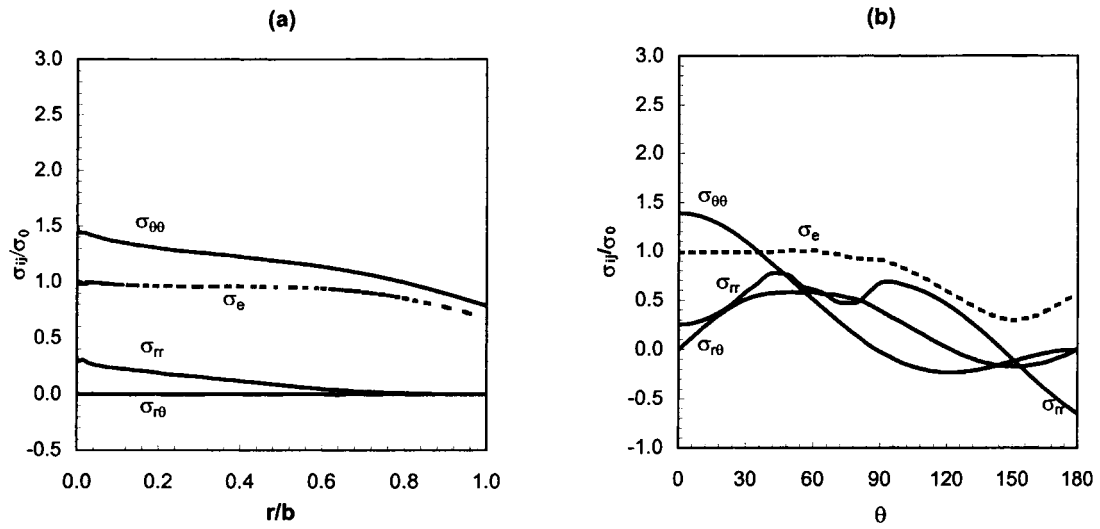

Fig. 8. Stress distributions of CCP specimen with $a/W = 0.5$ and $L/W = 3$ for uniformly distributed limit load $P = 1.0P_L$. (a) Radial distribution of stresses along the uncracked ligament, (b) angular distribution of stresses at $r = 0.05b$.

rigid displacement for large deformation levels or the limit load case. The rectangular and polar coordinate systems at the crack tip are illustrated in Fig. 2(a).

3.1. Effect of deformation level

Fig. 6(a) and (b) are the radial distributions of the stress components along the remaining ligament and the angular variations of stresses at $r = 0.0005b$ from the crack tip, respectively, for a low applied

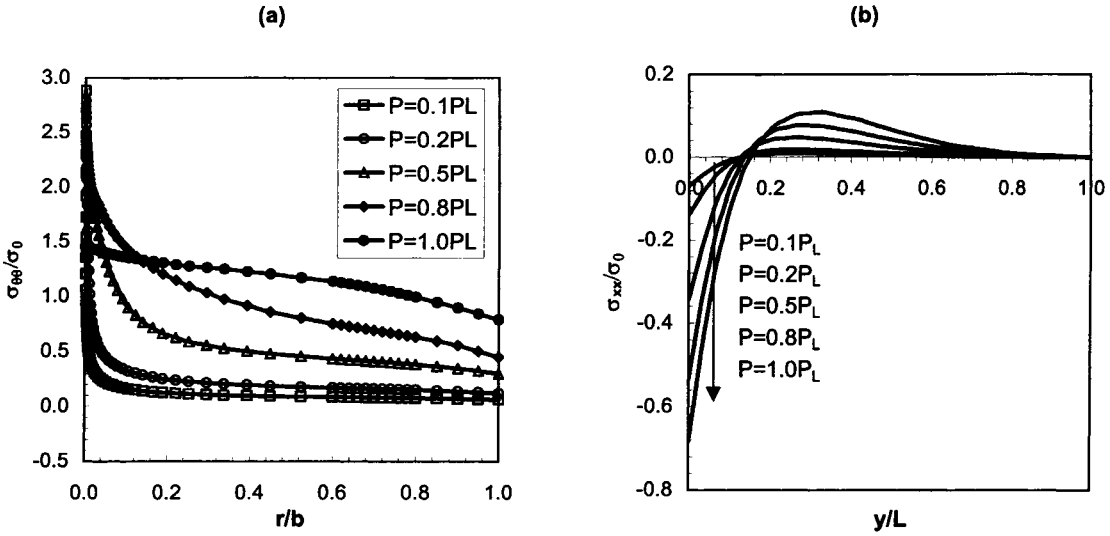

Fig. 9. Comparison of stress variations of CCP specimen with $a/W = 0.5$ and $L/W = 3$ for several uniformly distributed load levels shown in figures. (a) Crack opening stress $\sigma_{\theta\theta}$ along the uncracked ligament, (b) normal stress σ_{xx} along the vertical centerline.

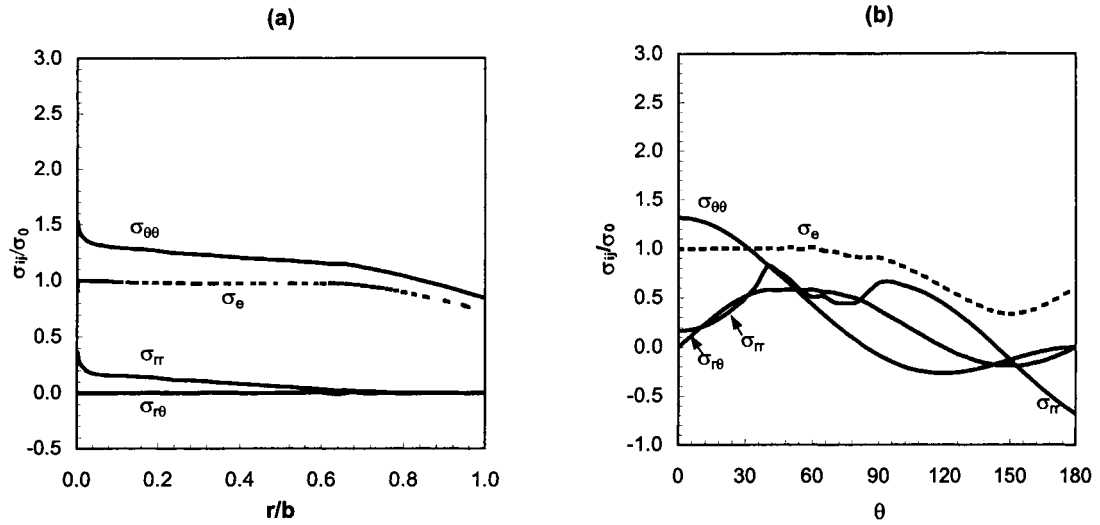

Fig. 10. Stress distributions of CCP specimen with $a/W = 0.5$ and $L/W = 3$ for uniformly rigid displacement at the limit load. (a) Radial distribution of stresses along the uncracked ligament, (b) angular distribution of stresses at $r = 0.05b$.

load $P = 0.1P_L$. As shown in Fig. 6(a), the stresses are small on the entire ligament; but when the crack tip is approached the crack opening stress $\sigma_{\theta\theta}$ ahead of the crack tip has a sharp increase and approximately attains the limiting value $2.97\sigma_0$ given by the Prandtl slip-line field (Prandtl, 1920). Moreover, the Mises effective stress σ_e is equal to σ_0 over almost the entire angular range around the crack tip as shown in Fig. 6(b). Comparing Fig. 6(b) with Fig. 5 of Hutchinson (1968) or Fig. 1 of Zhu and Chao (1999), it can be concluded that under small scale yielding the crack-tip field of CCP is the Prandtl field, which is in agreement with Shih and German (1981).

Fig. 7(a) and (b) depict stress distributions along the uncracked ligament and around the crack tip at $r = 0.05b$, respectively, for an applied load $P = 0.8P_L$. At this deformation level, (i) the stresses σ_{rr} and $\sigma_{\theta\theta}$ at the crack tip ($r \to 0$, $\theta = 0^\circ$) decrease, (ii) the tensile stress $\sigma_{\theta\theta}$ on the ligament (finite r, $\theta = 0^\circ$) increases, relative to the corresponding stress for $P = 0.1P_L$, (iii) compressive stress σ_{rr} occurs near the crack face ($\theta = 180^\circ$) and (iv) an elastic sector (i.e. the region with $\sigma_e < \sigma_0$) appears in $100^\circ < \theta \leq 180^\circ$. At the limit load P_L of CCP, stress distributions along the ligament and around the crack tip at $r = 0.05b$ are illustrated in Fig. 8(a) and (b), respectively. These figures show that the stresses at the crack tip decrease further and the compressive stress σ_{rr} on the crack face increases as the applied load increases. However, the tensile stress $\sigma_{\theta\theta}$ on the ligament is only close, but by no means equal, to a uniform value with $\sigma_{\theta\theta}$ being slightly higher towards the crack tip. The elastic sector near the crack face happens in $70^\circ < \theta \leq 180^\circ$. All stresses in the plastic region, $0^\circ \leq \theta \leq 45^\circ$, are close to the slip-line field given by (1).

Fig. 9(a) and (b) show the comparisons of the stress distributions along the ligament and along the vertical centerline (V-line) for several different applied loads ($P = 0.1P_L$, $P = 0.2P_L$, $P = 0.5P_L$, $P = 0.8P_L$ and $P = 1.0P_L$). From Fig. 9(a), one can see that the crack opening stress gradually decreases at the crack tip but increases along the ligament as the applied load increases. This mechanics behavior of CCP is consistent with that in a low hardening material with $n = 10$ (c.f. Figures 8 and 9 in O'Dowd and Shih, 1992). As a result, the constraint of the crack tip decreases gradually with increasing load. Fig. 9(b) reveals that both tensile and compressive stresses on the V-line increase as applied load increases. Thus a bending moment M_{VL} that is the resultant of stress σ_{xx} on V-line increases as the

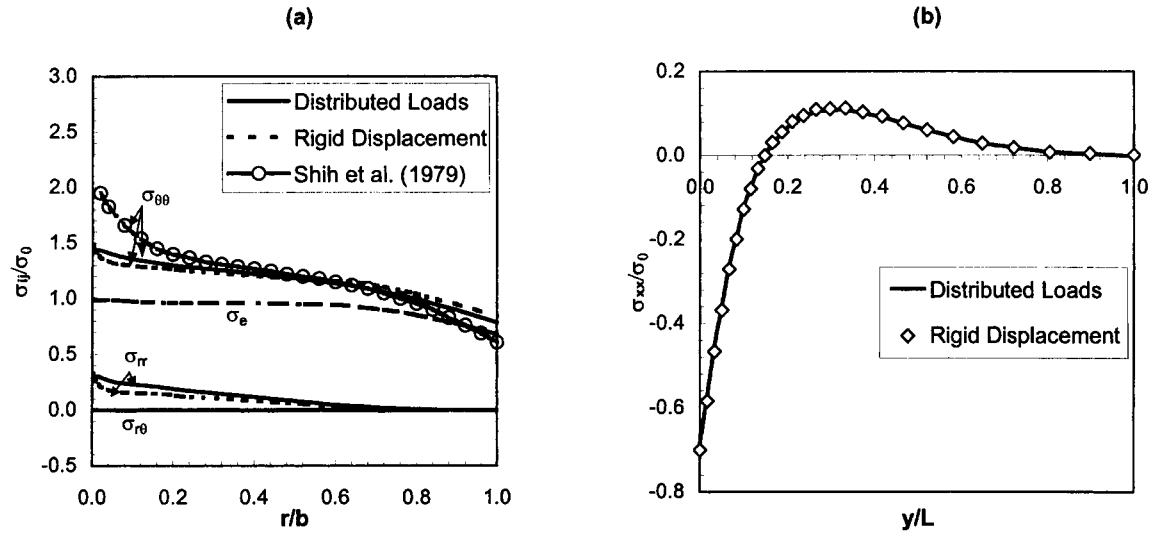

Fig. 11. Comparison of stress variations for CCP specimen with $a/W = 0.5$ and $L/W = 3$ under uniformly distributed loads and rigid displacement at the limit load. (a) Stresses along the uncracked ligament, (b) normal stress σ_{xx} along the vertical centerline.

applied load increases. At the limit load, it can be calculated that $M_{VL} = 0.5357abB\sigma_0$ from the results shown in Fig. 9(b). For uniformly distributed loads the resultant moment M_{top} acting on the top edge about the mid-ligament of CCP is $p_L aWB/2$. In terms of uniformly distributed load $p_L = P_L/(2WB)$ and formula (2), we have

$$M_{top} = a(W-a)B\sigma_0/\sqrt{3} \approx 0.5774abB\sigma_0 \tag{3}$$

On the remaining ligament, therefore, there exists a counter-clockwise moment $M_{top} - M_{VL} = 0.0416abB\sigma_0$ about the mid-ligament. It appears that it is this moment that makes the crack opening stress $\sigma_{\theta\theta}$ on the ligament non-uniform and larger at the crack tip ($r \to 0$) than at the external boundary ($r \to b$), as shown in Fig. 8(a). This result corroborates the prediction in Section 2 and provides support for why the numerical results at the limit state deviate somewhat from the slip-line field (1).

3.2. Effect of loading type

At the limit load, for the case of uniformly distributed applied load the numerical results have been given in Fig. 8. For the case of applied rigid displacement, the stress distributions from FEA are shown in Fig. 10(a) and (b). Comparison of stress variations along the remaining ligament and along the V-line is shown in Fig. 11 for the two loading types. It is shown that the FEA results are almost the same for the two loading cases. In Fig. 11(a) numerical results of the tensile stress $\sigma_{\theta\theta}$ from Shih et al. (1979) are also shown. It can be seen that our FEA results for the two loading types are closer to the slip-line field (1). In Fig. 11(b) the tensile and compressive stresses along the V-line, thus the equivalent moment M_{VL}, are slightly larger for the case of rigid displacement than for the case of uniformly distributed loads. Using the FEA results, it can be determined that the resultant moments $M_{VL} = 0.5408abB\sigma_0$, $M_{top} = 0.5759abB\sigma_0$, $M_{top} - M_{VL} = 0.0351abB\sigma_0$ for the displacement case and $M_{VL} = 0.5357abB\sigma_0$, $M_{top} = 0.5773abB\sigma_0$, $M_{top} - M_{VL} = 0.0416abB\sigma_0$ for the distributed load case. Thus, the moment difference ($M_{top} - M_{VL}$) acting on the uncracked ligament about the mid-ligament for the rigid displacement case is indeed less than that for the distributed load case. Accordingly, the tensile stress $\sigma_{\theta\theta}$ along the

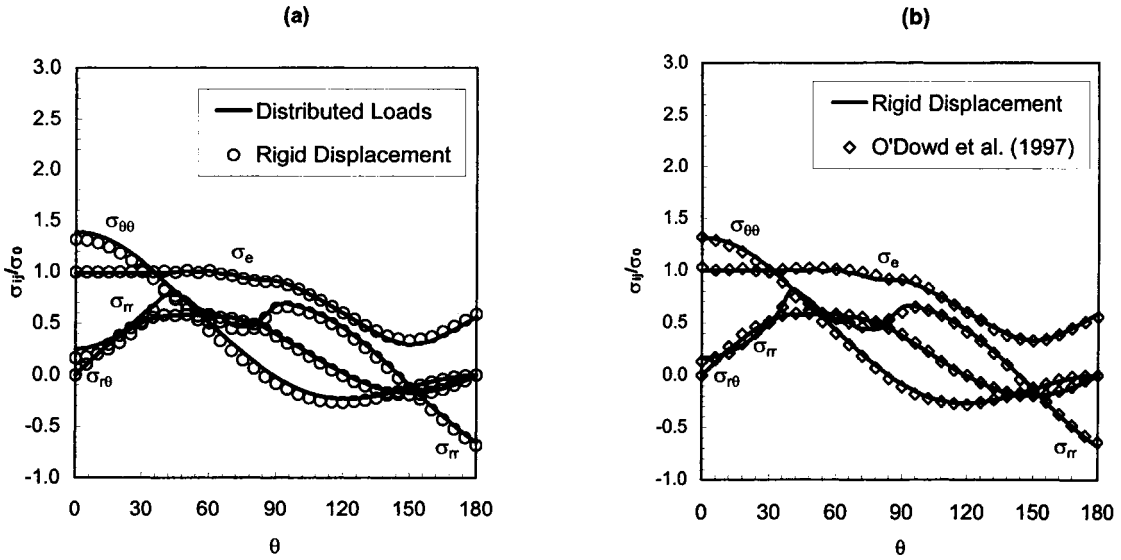

Fig. 12. Comparison of angular stress variations for CCP specimen with $a/W = 0.5$ and $L/W = 3$ at $r = 0.05b$ at the limit load. (a) Comparison between two loading types, (b) comparison between this paper and O'Dowd et al. (1997).

uncracked ligament is relatively flat in the rigid displacement case, as shown in Fig. 11(a). This conclusion corroborates our prediction in Section 2.

The numerical comparison in Fig. 12(a) shows that the angular variations of stresses are nearly the same for the two loading cases. Fig. 12(b) indicates that our FEA results are in very good agreement with those of O'Dowd et al. (1997), thus giving confidence about the present FEA calculations and results.

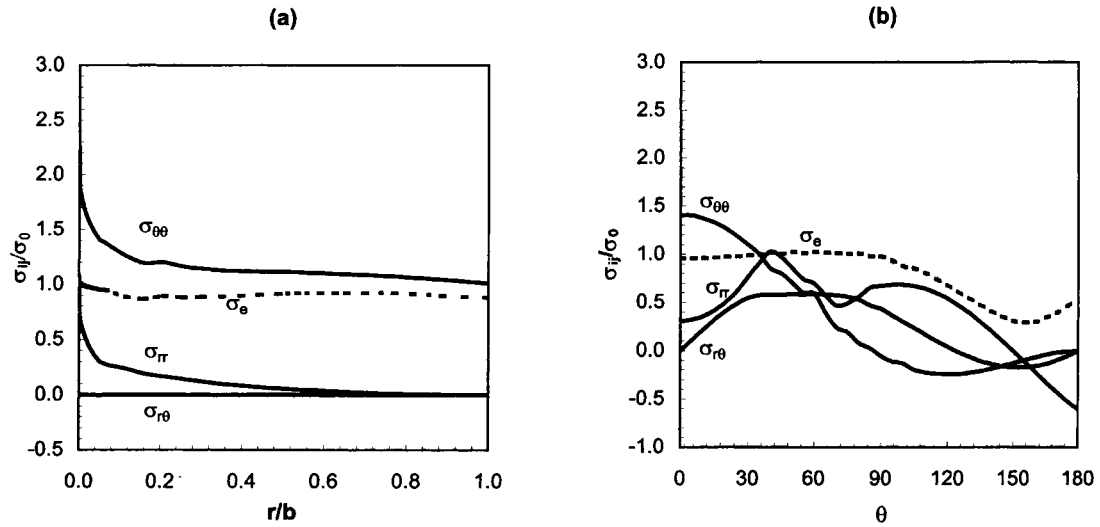

Fig. 13. Stress distributions of CCP specimen with $a/W = 0.1$ and $L/W = 3$ at the limit load. (a) Radial distribution of stresses along the uncracked ligament, (b) angular distribution of stresses at $r = 0.05b$.

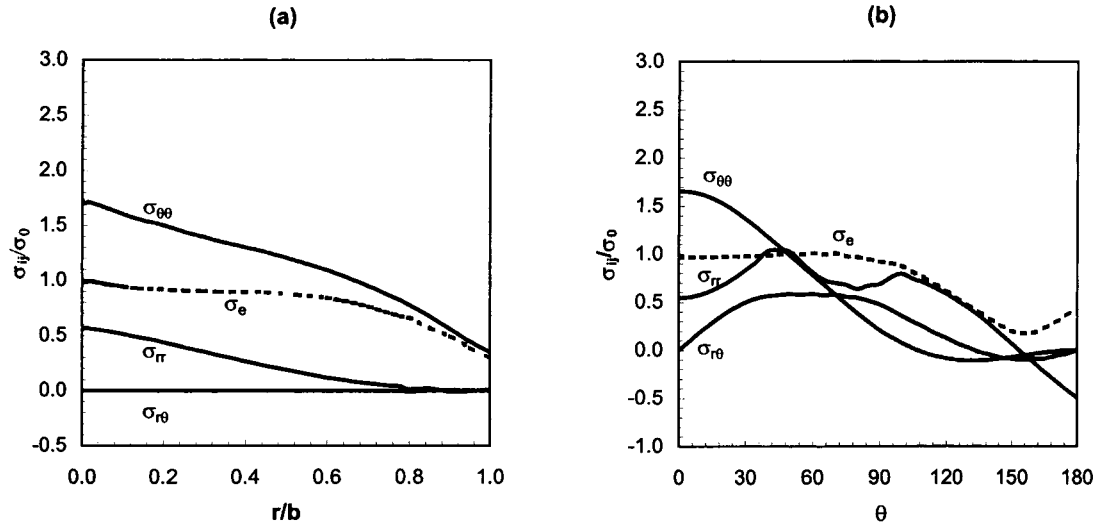

Fig. 14. Stress distributions of CCP specimen with $a/W = 0.9$ and $L/W = 3$ at the limit load. (a) Radial distribution of stresses along the uncracked ligament, (b) angular distribution of stresses at $r = 0.05b$.

3.3. Effect of crack depth (a/W)

Figs. 10, 13 and 14 illustrate the radial distributions of stresses along the remaining ligament and angular variations of stresses around the crack tip at $r = 0.05b$ for the crack depth $a/W = 0.5$, 0.1 and 0.9 at the limit load, respectively. For the three cracks, the angular variations of stresses around the crack tip and the size of elastic sector near the crack face are similar. Fig. 15(a) indicates that except for

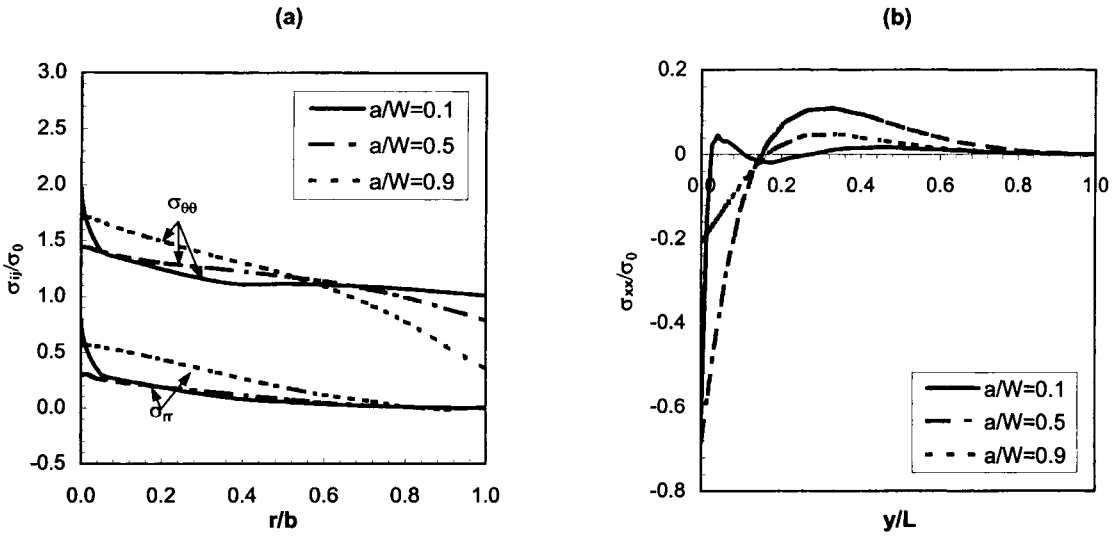

Fig. 15. Comparison of stress variations of CCP specimen with $L/W = 3$ for $a/W = 0.1$, 0.5, 0.9 at the limit load. (a) Stresses along the uncracked ligament, (b) normal stress σ_{xx} along the vertical centerline.

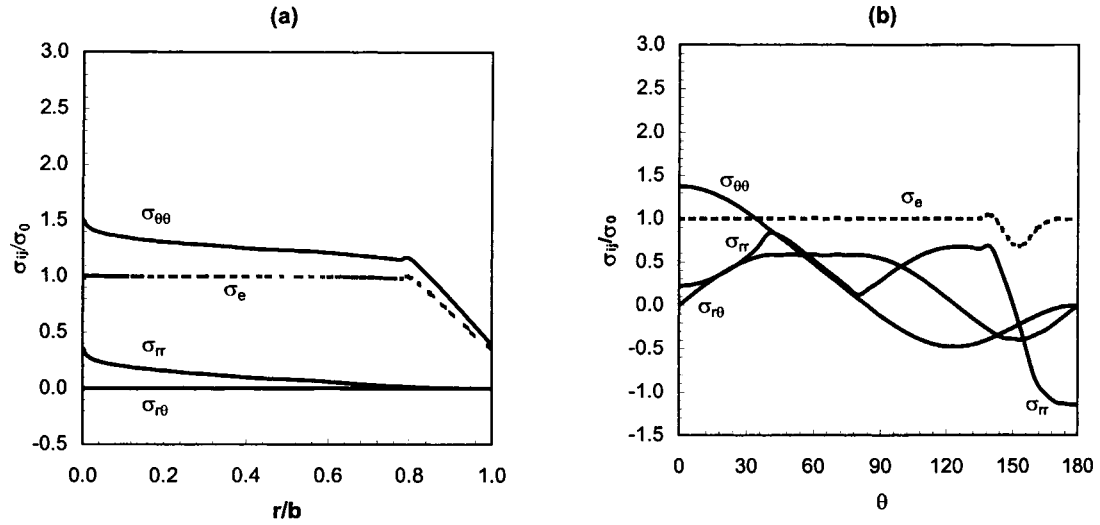

Fig. 16. Stress distributions of CCP specimen with $a/W = 0.5$ and $L/W = 0.75$ at the limit load. (a) Radial distribution of stresses along the uncracked ligament, (b) angular distribution of stresses at $r = 0.05b$.

the immediate vicinity of the crack tip, the stress distributions along the uncracked ligament are close to the values of the slip-line field (1) for the shallow crack $a/W = 0.1$, but deviate for the deep crack $a/W = 0.9$. The stress variations for $a/W = 0.5$ are between those for $a/W = 0.1$ and $a/W = 0.9$. Using the normal stress σ_{xx} along the V-line as plotted in Fig. 15(b), the equivalent bending moment are determined as $M_{VL} = 0.5689abB\sigma_0$, $0.5408abB\sigma_0$, $0.3095abB\sigma_0$ for $a/W = 0.1$, 0.5 and 0.9, respectively. Then from the moment M_{top}, we obtain $(M_{top} - M_{VL}) = 0.0082abB\sigma_0$, $0.0351abB\sigma_0$, $0.2618abB\sigma_0$ on the ligament about the mid-ligament for the three cracks. The magnitudes of these moments determine the

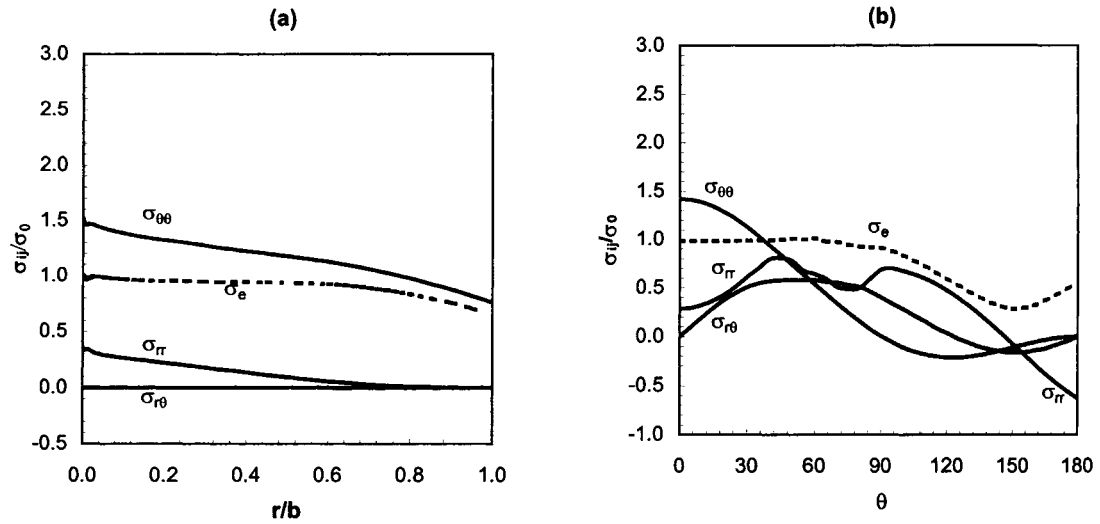

Fig. 17. Stress distributions of CCP specimen with $a/W = 0.5$ and $L/W = 10$ at the limit load. (a) Radial distribution of stresses along the uncracked ligament, (b) angular distribution of stresses at $r = 0.05b$.

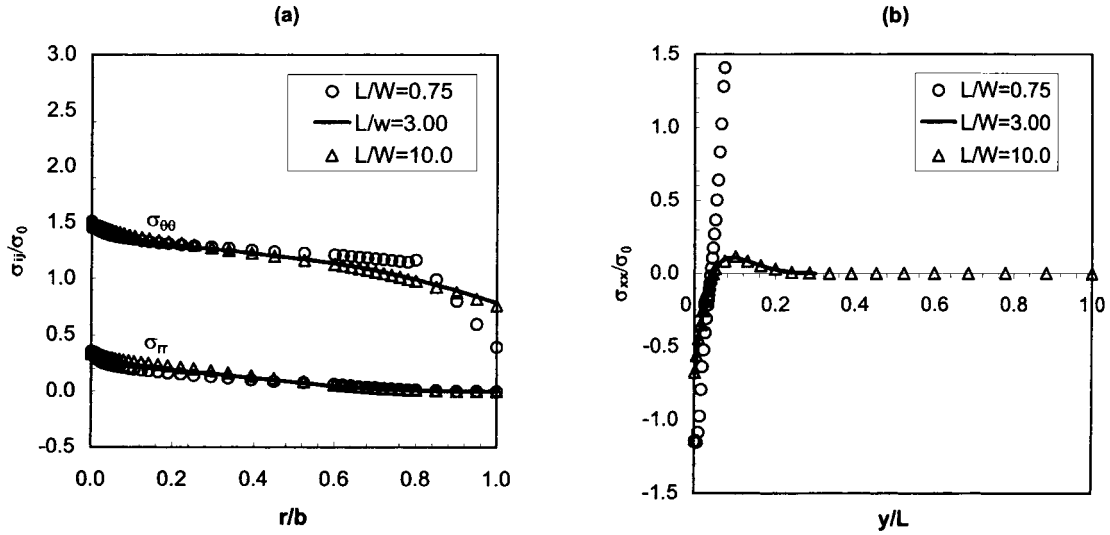

Fig. 18. Comparison of stress variations of CCP specimen with $a/W = 0.5$ for $L/W = 0.75$, 3, 10 at the limit load. (a) Stresses along the uncracked ligament, (b) normal stress σ_{xx} along the vertical centerline (Note: the scale y is normalized by $L = 10W$).

extent of uniformity of the stress distributions in Fig. 15(a). It should be noted that the CCP slip-line field (1) corresponds to $(M_{top}-M_{VL}) = 0$ so that the opening stress on the ligament has to be uniform. Our FEA results are non-uniform on the ligament, which can be attributed to the reason that $(M_{top}-M_{VL}) > 0$ for all crack depths. However, in the limit of $a/W \to 0$, our calculations show the moment $(M_{top}-M_{VL})$ approaches zero so that the stresses on the ligament approach to the slip-line field (1). With increasing crack depth the moment $(M_{top}-M_{VL})$ becomes larger; accordingly the tensile stress on the ligament deviates from the slip-line field (1) further and the crack opening stress (or constraint) increases near the crack tip for CCP.

3.4. Effect of specimen length (L/W)

Leevers and Radon (1982), Lei and Neale (1997) pointed out that when specimen length is at lease twice the specimen width (i.e. $L/W \geq 2$) for a CCP in elastic materials, the stress intensity factor, the stress biaxiality ratio and the crack-tip stresses are independent of specimen length. To explore the effect of L/W on the crack-tip fields for CCP in perfectly plastic materials, we choose $L/W = 0.75$, 3 and 10 to perform FEA calculations with $a/W = 0.5$. Figs. 16, 10 and 17 depict the radial distributions of stresses on the remaining ligament and the angular variations of stress components at $r = 0.05b$ for the three specimens at the limit load, respectively. Comparing Figs. 16(b), 10(b) and 17(b), one can find that the angular variations of stresses are nearly the same for the long specimens with $L/W = 3$ and $L/W = 10$. Comparing to the short specimen with $L/W = 0.75$, the difference in angular variation of stresses for the two long specimens occurs only over $60^\circ \leq \theta \leq 180^\circ$. For all three specimens, compressive stress σ_{rr} occurs on the crack face at limit load. However, only the compressive stress for $L/W = 0.75$ attains yielding state near the crack face, the other two stay in the elastic state.

Comparison of stresses in Fig. 18(a) shows that (i) the stress distributions on the uncracked ligament are identical for the two long specimens, and (ii) the opening stress $\sigma_{\theta\theta}$ on the ligament for the short specimen is nearly the same as those of the long specimens in $0 \leq r/b \leq 0.6$ but different in $0.6 < r/b \leq 1.0$. The normal stresses σ_{xx} on the V-line as shown in Fig. 18(b) are identical and close to zero

near the top edge for the two long specimens, but they are quite different from those for the short specimen. For the short specimen, the stresses σ_{xx} along V-line exceed the yield strength in the regions near the crack face and near the top edge. Thereby, a compressive yielding zone and a tensile yielding zone occur simultaneously in these two regions. This finding from our FEA is consistent with the experimental observation of Quirk and Bevitt (1991).

Using the normal stresses in Fig. 18(b), we obtain the resultant moment $M_{VL} = 0.5278abB\sigma_0$ for the short specimen and $M_{VL} = 0.5408abB\sigma_0$ for the two long specimens. Then from the moment M_{top}, one obtains the moment $M_{top}-M_{VL} = 0.0457abB\sigma_0$ for the short specimen and $M_{top}-M_{VL} = 0.0351abB\sigma_0$ for the long specimens. Because this moment $(M_{top}-M_{VL})$ is larger for the short specimen than for the long specimens, the opening stress $\sigma_{\theta\theta}$ along the ligament for the short specimen deviates more from the uniform slip-line field as shown in Fig. 18(a). On the other hand, the stress σ_{xx} on the V-line shown in Fig. 18(b) is close to zero when $y/L \geq 0.24$ (i.e., $y \geq 2.4W$ or $L \geq 2.4W$) for both $L/W = 3$ and $L/W = 10$. Also from Fig. 15(b), the stress σ_{xx} vanishes as $y/L \geq 0.8$ (i.e., $y \geq 2.4W$ or $L \geq 2W$). Therefore, it may be concluded that when $L \geq 2.4W$ (or roughly $L \geq 2W$) the crack-tip stress field and constraint are independent of the specimen length L/W for CCP.

4. Fully plastic crack-tip field of DECP specimen

In this section, we report our FEA results for the DECP specimen. Since there are many similarities between CCP and DECP, we only report results for the effects of deformation level and crack depth on the crack-tip stress fields or constraint. The close-form formulae of limit load are first discussed for the DECP specimen with different crack depths; FEA results are then presented with special attention on under what conditions the crack-tip stress field can approach the Prandtl slip-line field (Prandtl, 1920). Unless specified otherwise, in this section the dimensions of DECP specimen are $a/W = 0.5$, $L/W = 3$, and loading type is the uniformly distributed load at the top edge. The rectangular and polar coordinate systems at the crack tip are illustrated in Fig. 3(a).

4.1. Limit load for different crack depths (a/W)

Since the slip-line field of DECP specimens depends on the crack depth (Ewing and Hill, 1967), several formulae of limit load for DECP are reported in various literatures. Based on theory of plasticity (c.f. Kachanov, 1974 and McClintock, 1971), the limit load from slip-line field of DECP with deep crack can be written as

$$P_L = \frac{4}{\sqrt{3}}\left(1+\frac{\pi}{2}\right)(W-a)B\sigma_0 \tag{4}$$

The limit load of DECP is also presented by Kumar et al. (1981), without any limitation, as the EPRI result (Note that Miller (1988) pointed out that (5) is not correct)

$$P_L = \left(0.72 + 1.82\frac{b}{W}\right)WB\sigma_0 \tag{5}$$

Ewing and Hill (1967) indicated that for deep cracks of $a/W > 0.884$ the slip-line field is restricted to the remaining ligament and is the well-known Prandtl field, whose limit load can be calculated by (4). For shallow cracks with $a/W \leq 0.884$, they represented the limit load as

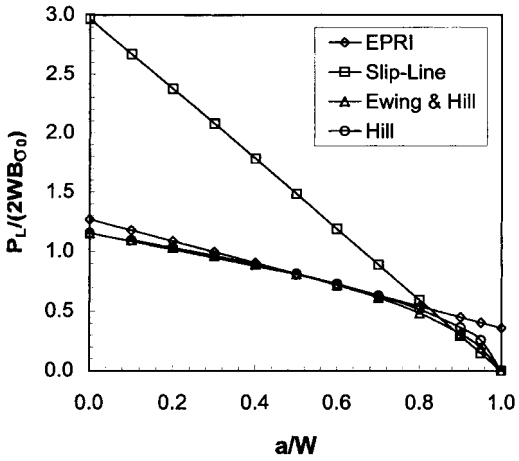

Fig. 19. Variations of different limit load formulae of DECP with the crack depth a/W.

$$P_L = \frac{4}{\sqrt{3}}\left[1 + \ln\left(1 + \frac{a}{2b}\right)\right](W-a)B\sigma_0 \tag{6}$$

and indicated that for small a/W the difference between (6) and Hill's approximate formula

$$P_L = \frac{4}{\sqrt{3}}\sqrt{1 - \frac{a}{W}}WB\sigma_0 \tag{7}$$

can be ignored (c.f. Wu, et al., 1990).

Fig. 19 plots the variations of the limit load determined from (4)–(7) with crack depth a/W. The straight line of limit load (4) intersects the curves of limit loads (5), (6) and (7) at $a/W = 0.825$, $a/W = 0.849$ and $a/W = 0.884$, respectively. The limit load (4) from the slip-line field with deep cracks could be invalid for 'shallow cracks' of $a/W \leq 0.825$. The value of limit load (5) from EPRI is higher than that of (4) for 'deep cracks' of $a/W \geq 0.825$ and gives a finite value when $a/W \to 1$. Therefore (5) could be invalid for these deep cracks. Fig. 19 indicates that for $a/W \leq 0.7$ there is indeed no difference between Ewing and Hill's limit load (6) and Hill's limit load (7). In the region of $0.4 \leq a/W \leq 0.7$, the three formulae of limit load (5), (6) and (7) are identical to each other. Our experience from FEA indicates only the smallest value of the four limit loads given in (4)–(7) can be attained for a specific crack. Therefore, one may argue that the valid range of the above limit loads (4), (5), (6) and (7) are $a/W \geq 0.884$, $0.4 \leq a/W \leq 0.7$, $a/W \leq 0.884$ and $a/W \leq 0.7$, respectively. For convenience, we adopt the limit load given by Ewing and Hill (1967), that is

$$P_L = \begin{cases} \dfrac{4}{\sqrt{3}}\left[1 + \ln\left(1 + \dfrac{a}{2b}\right)\right](W-a)B\sigma_0, & a/W \leq 0.884 \\ \dfrac{4}{\sqrt{3}}\left(1 + \dfrac{\pi}{2}\right)(W-a)B\sigma_0, & a/W \geq 0.884 \end{cases} \tag{8}$$

4.2. Effect of deformation level

Under small-scale yielding, the discussion in Section 3.1 indicates that the crack-tip field of CCP is the

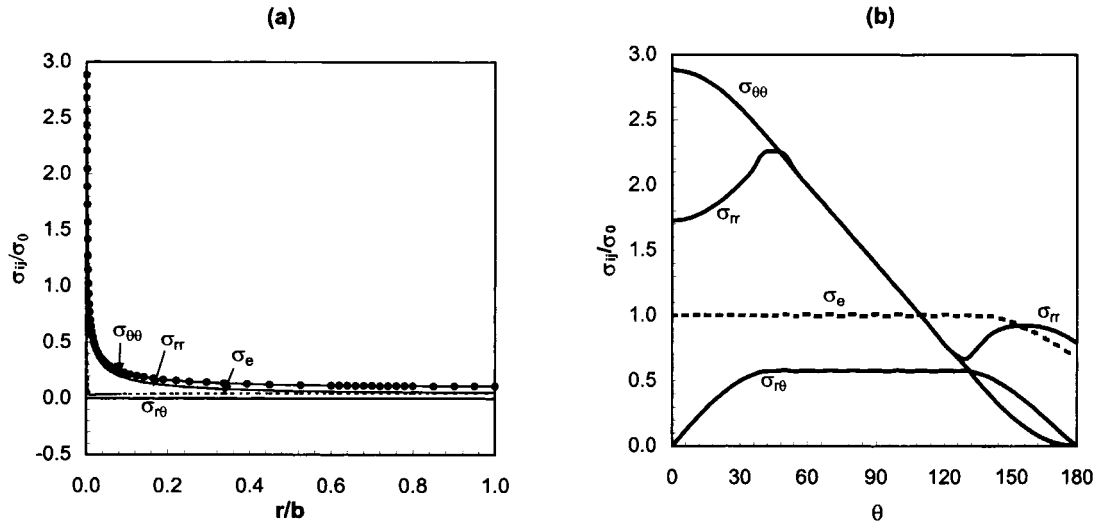

Fig. 20. Stress distributions of DECP specimen with $a/W = 0.5$ and $L/W = 3$ for uniformly distributed load $P = 0.1P_L$. (a) Radial distribution of stresses along the uncracked ligament, (b) angular distribution of stresses at $r = 0.0005b$.

Prandtl field. This conclusion is also valid here for DECP under very small applied load. Fig. 20(a) and (b) are the radial distributions of stresses along the remaining ligament and the angular variations of stresses at $r = 0.0005b$ from the crack tip for DECP with $a/W = 0.5$ and small applied load $P = 0.1P_L$. Fig. 20(a) shows again that the stresses are small on the entire uncracked ligament, but when the crack tip is approached the tensile stress $\sigma_{\theta\theta}$ ahead of the crack tip has a sharp increase and approximately attains the limit value $2.97\sigma_0$ of the Prandtl field. Moreover, the angular stress distribution in Fig. 20(b) is approximately the Prandtl field. With increasing applied loads the mechanics

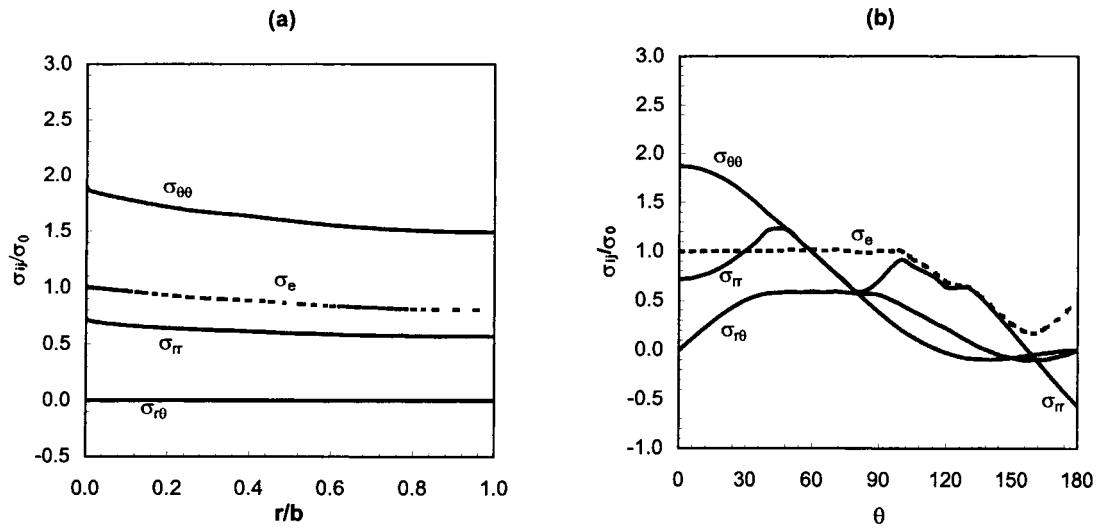

Fig. 21. Stress distributions of DECP specimen with $a/W = 0.5$ and $L/W = 3$ at the limit load. (a) Radial distribution of stresses along the uncracked ligament, (b) angular distribution of stresses at $r = 0.05b$.

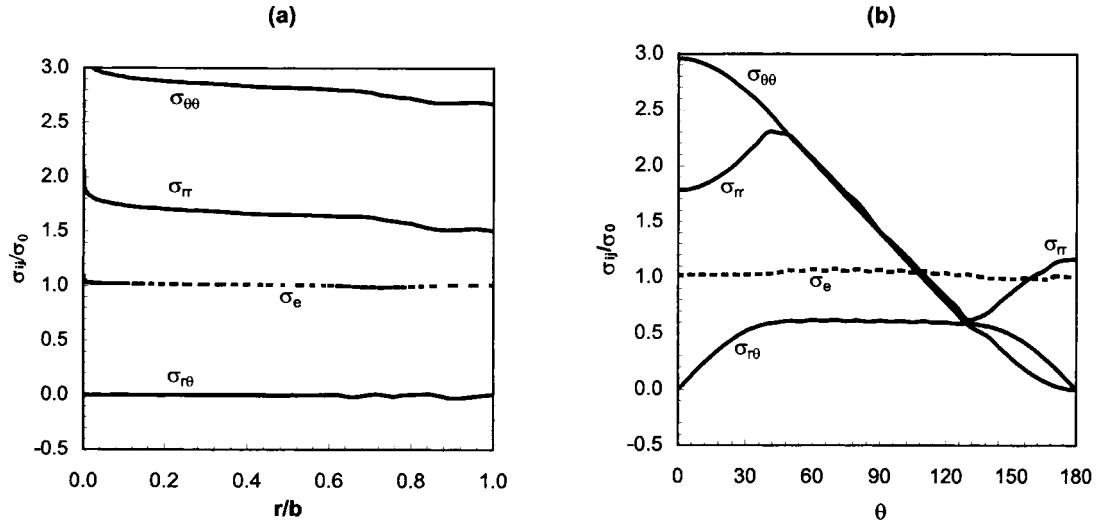

Fig. 22. Stress distributions of DECP specimen with $a/W = 0.95$ and $L/W = 3$ at the limit load. (a) Radial distribution of stresses along the uncracked ligament, (b) angular distribution of stresses at $r = 0.05b$.

behavior of DECP is similar to that for CCP in that the stresses along the ligament decrease only at the crack tip but increase on the entire ligament. At the limit load (8), the distributions of stress components are depicted in Fig. 21(a) and (b), respectively, along the ligament and around the crack tip at $r = 0.05b$. Note that (i) an elastic sector exists in the interval of $100^\circ < \theta \leq 180^\circ$, (ii) a compressive stress σ_{rr} occurs near the crack face, and (iii) the stress distributions along the ligament are non-uniform. Comparing of Fig. 20 and Fig. 21, one sees that the tensile stress or constraint immediately ahead of the crack tip for DECP decreases with increasing load.

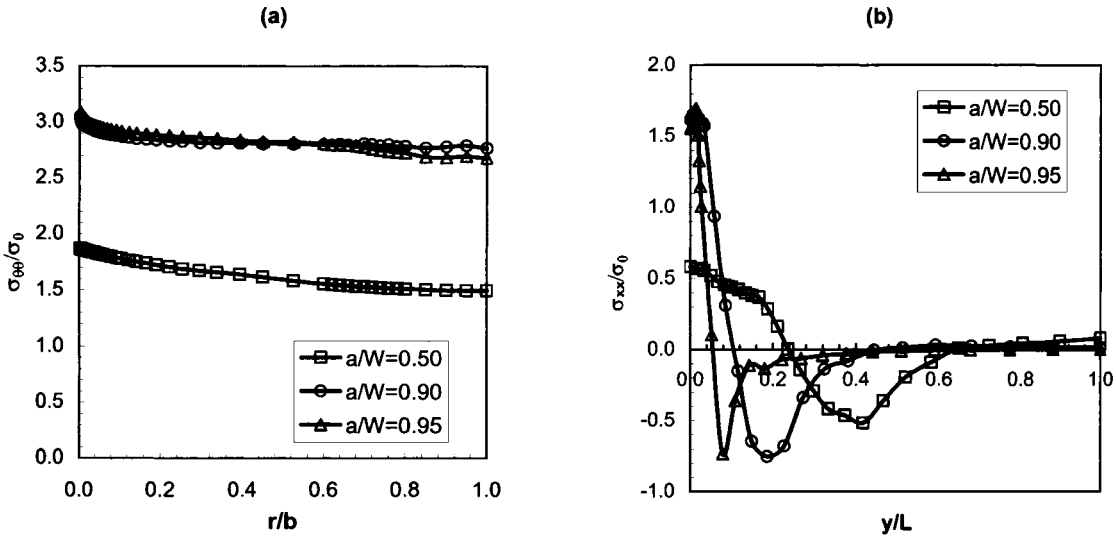

Fig. 23. Comparison of stress variations of DECP specimen with $L/W = 3$ for $a/W = 0.5$, 0.9, 0.95 at the limit load. (a) Crack opening stress $\sigma_{\theta\theta}$ along the uncracked ligament, (b) normal stress σ_{xx} along the vertical centerline.

4.3. Effect of crack depth (a/W)

Analyses in Section 4.1 and results in Fig. 19 show that the limit load of DECP depends on the crack depth a/W. Fig. 21 shows the numerical results of DECP for the crack of $a/W = 0.5$ at the limit load. For the deep crack of $a/W = 0.95$, the radial distributions of stresses along the ligament and angular stress variations around the crack tip at $r = 0.05b$ are illustrated in Fig. 22 at the limit load by (8). The stresses on the entire ligament attain the yielding state for this deep crack because Mises equivalent stress σ_e is equal to σ_0 anywhere along the ligament. The crack tip is completely enclosed by plastic sectors and consequently the angular variations of stresses resemble the Prandtl field. This is consistent with the conclusion of Ewing and Hill (1967) on the slip-line field of DECP. For $a/W = 0.9$, stress distributions are almost the same as those for $a/W = 0.95$, but an elastic sector exists in about $170^\circ < \theta < 180^\circ$ so that the crack-tip stress field is 'slightly' different from that for $a/W = 0.95$. As can be seen from Fig. 21(b) and Fig. 22(b), the behavior of $a/W = 0.9$ is indeed a transition form 'shallow' to 'deep' cracks for DECP specimen. The transition at $a/W = 0.9$ is very close to the predicted value at $a/W = 0.884$ by Ewing and Hill (1967) and is identical to the transition value obtained by Betegon and Hancock (1991) for DECP specimen in low hardening materials.

Fig. 23 shows the comparison of the tensile stress $\sigma_{\theta\theta}$ along the uncracked ligament and the normal stress σ_{xx} along the V-line for $a/W = 0.5$, 0.9 and 0.95. As shown in Fig. 23(a), the tensile stress distributions along the remaining ligament are nearly identical for the two deep cracks of $a/W = 0.9$ and $a/W = 0.95$, but are different from those for the shallow crack of $a/W = 0.5$. The variations of stress σ_{xx} along the V-line are different for the three cracks, as shown in Fig. 23(b). From these stresses, the moment M_{VL} is determined to be $0.7869abB\sigma_0$, $1.4744abB\sigma_0$ for $a/W = 0.5$, 0.9 and 0.95, respectively. On the top edge, at the limit load (8) the resultant moment of DECP about mid-ligament for the uniformly distributed loads can be written as

$$M_{top} = \begin{cases} \dfrac{1}{\sqrt{3}}\left[1 + \ln\left(1 + \dfrac{a}{2b}\right)\right] abB\sigma_0, & a/W \le 0.0884 \\ \dfrac{1}{\sqrt{3}}\left(1 + \dfrac{\pi}{2}\right) abB\sigma_0, & a/W \ge 0.884 \end{cases} \tag{9}$$

From (9), $M_{top} = 0.8114abB\sigma_0$ for $a/W = 0.5$ and $M_{top} = 1.4842abB\sigma_0$ for both $a/W = 0.9$ and $a/W = 0.95$. Thus a counter-clockwise moment $M_{top} - M_{VL} = 0.025abB\sigma_0$, $0.010abB\sigma_0$, $0.022abB\sigma_0$ acts respectively on the uncracked ligament about the mid-ligament for the three cracks. These moments are small but by no means zero. Therefore, the opening stresses for the deep cracks are close to the uniform value of the Prandtl field on the entire remaining ligament. The results shown in Fig. 23(b) also indicate that as $y/L \ge 0.65$ (i.e. $y \ge 1.95W$ or $L \ge 2W$), the crack-tip field is independent of the specimen length L/W for DECP specimens.

5. Summary and conclusions

Detailed finite element analyses are performed for the CCP and DECP subjected to far field tension in non-hardening materials under plane strain conditions. The analyses are based on the small-strain formulations and the J_2 flow theory associated with the von Mises yield rule for perfect plasticity. Based on the present analyses and results, the following conclusions can be made:

1. At load levels under ten percent of the limit load, i.e. under small scale yielding, the plastic zone near the crack tip is very small and the crack-tip stress field is the Prandtl field for both CCP and DECP.

As the deformation level increases, the crack opening stress and constraint level at the crack tip decrease for CCP of all crack depths and for DECP specimens of shallow cracks. At the limit load, the stresses of CCP on the uncracked ligament approach the slip-line field. For DECP with sufficiently deep cracks (e.g. $a/W \geq 0.95$), the crack-tip constraint level remains 'nearly' constant for all deformation levels and the crack-tip field is approximately the Prandtl field.

2. The crack depth has certain effects on the crack-tip field of CCP. At the limit load, the tensile stress and constraint ahead of the crack tip increase gradually as a/W increases, and the crack-tip field is almost the same as the CCP slip-line field in the plastic region $0^\circ \leq \theta \leq 45^\circ$ for all cracks of $a/W \leq 0.5$. In contrast, the crack depth has considerable effects on the crack-tip field for DECP. At the limit load, the crack opening stresses on the entire ligament for shallow cracks are much smaller than those for deep cracks in a DECP. The crack-tip field is the Prandtl field for the deep cracks of $a/W \geq 0.95$ but slightly different for $a/W = 0.9$. And the crack depth $a/W = 0.9$ is indeed the transition between deep and shallow cracks of DECP. This transition value matches well with the result of slip-line analyses by Ewing and Hill (1967) and is identical to that of Betegon and Hancock (1991) for low hardening materials.
3. There is a vertical symmetrical centerline (V-line) for both CCP and DECP specimens. Effect of specimen length on the crack-tip fields can be determined by the variations and magnitude of stresses on the V-line. For short specimens (e.g. $L/W = 0.75$), the stress σ_{xx} appears along the whole V-line, and a tensile and a compressive yielding region occur near the top and bottom of V-line, respectively, at the limit load. This was observed experimentally by Quirk and Bevitt (1991). For long specimens (e.g. $L/W \geq 3$), only a portion of the V-line develops by σ_{xx} and there is no σ_{xx} acting on the V-line near the top edge. When $L/W \geq 2.4$ (or roughly $L/W \geq 2$) for CCP and $L/W \geq 2$ for DECP, the crack-tip stresses are independent of the specimen length.
4. At the limit load, the crack face is under compression for all cracked CCP and only for shallow cracked DECP. For deep cracked DECP, the crack face is under tension. For CCP specimens, the largest compressive stress along the V-line is at the crack face and the stress σ_{xx} along the ligament is close to zero. For DECP specimens, however, the largest tensile stress along the V-line exists at the ligament and the stress σ_{xx} along the ligament is much larger than zero.
5. When the specimens are loaded by remote tension, horizontal tensile and compressive stresses develop simultaneously along the V-line of CCP and DECP and result in a bending moment M_{VL} that decreases the magnitude of stresses ahead of the crack tip. On the top edge of specimen, the applied loads generate a moment M_{top} about the mid-ligament that increases the magnitude of stresses ahead of the crack tip. The moment difference (M_{top}–M_{VL}) on the ligament about the mid-ligament is generally small, but larger than zero for both CCP and DECP. Accordingly, the tensile stresses $\sigma_{\theta\theta}$ along the ligament are only close to be uniform, but not exactly uniform for these specimens. The experimental analyses of Quirk and Bevitt (1991) showed that it is due to this moment M_{VL} on the V-line, stable crack growth can occur in CCP specimen. The reason appears to be that an increasing moment M_{top} can be balanced by the increasing bending moment M_{VL} as the crack grows. As such, stable crack growth can be continued until the normal stress σ_{xx} along V-line attains a limiting condition.
6. For CCP specimens, the limit load is represented by (2). For DECP specimens, however, the limit load has different forms as expressed by (4)–(7). Our FEA results indicate that the limit load formula (5) of EPRI (Kumar et al., 1981 and Anderson, 1995) is valid only in the range of $0.4 \leq a/W \leq 0.7$, and the limit load formula (8) given by Ewing and Hill (1967) can be used for analyses of DECP specimens with any crack depth.

Two loading types are adopted in this work. The first is uniformly distributed applied loads and the second is uniform rigid displacement. At the limit load, the FEA results converge easier using the first

loading than using the second. Crack-tip field is closer to the slip-line field for the first loading than for the second, but the differences are small.

We would like to conclude the current paper with a brief discussion on quantifying the constraint level for CCP and DECP. It is demonstrated by Zhu and Chao (1999) that a three-term solution can be used to quantify the constraint at a crack tip by use of the parameter A_2. The three-term solution can be written as

$$\frac{\sigma_{ij}}{\sigma_0} \cong \tilde{\sigma}_{ij}^{\mathrm{Prandtl}}(\theta) + A_2\tilde{\sigma}_{ij}^{(2)}(\theta, n=30) + A_2^2\tilde{\sigma}_{ij}^{(3)}(\theta, n=30) \tag{10}$$

where $\tilde{\sigma}_{ij}^{\mathrm{Prandtl}}(\theta)$ is the Prandtl stress field, $\tilde{\sigma}_{ij}^{(2)}(\theta,n=30)$ and $\tilde{\sigma}_{ij}^{(3)}(\theta,n=30)$ are the second and third term angular stress functions of a low hardening material $n=30$ (Chao and Zhang, 1997). Eq. (10) can be used approximately to model the crack-tip stress field of any specimens in non-hardening materials for any deformation level. Using (10) to match with the present FEA stress results near the crack tip for CCP and DECP specimens, e.g. $\sigma_{\theta\theta}$ at $\theta=0^\circ$, the constraint parameter A_2 can be solved for different a/W. Having the A_2 value determined for a specific specimen and loading level, the angular variations of the stress components and hydrostatic stress (constraint) with a/W can then be predicted by (10). This is of course beyond the scope of the current paper; but can be done without much difficulty.

Acknowledgements

The authors appreciate the support of this work by NSF through NSF/EPDCoR Cooperative Agreement No.-9630167.

References

Betegon, C., Hancock, J.W., 1991. Two-parameter characterization of elastic-plastic crack-tip fields. Journal of Applied Mechanics 58, 104–110.

Chao, Y.J., Yang, S., Sutton, M.A., 1994. On the fracture of solids characterized by one or two parameters: theory and practice. Journal of the Mechanics of Physics and Solids 42, 629–647.

Chao, Y.J., Zhang, L., 1997. Tables of plane strain crack tip fields: HRR and higher order terms, ME-Report, 97–1, Department of Mechanical Engineering, University of South Carolina.

Chao, Y.J., Zhu, X.K., 1998. J-A_2 Characterization of crack-tip fields: extent of J-A_2 dominance and size requirements. International Journal of Fracture 89 (3), 285–307.

Ewing, D.J.F., Hill, R., 1967. The plastic constraint of V-notched tension bars. Journal of the Mechanics and Physics of Solids 15, 115–121.

Goldman, N.L., Hutchinson, J.W., 1975. Fully plastic crack problems: the center-cracked strip under plane strain. International Journal of Solids and Structures 11, 575–591.

Hancock, J.W., Reuter, W.G., Parks, D.M., 1993. Constraint and toughness parameterized by *T*. In: Constraint Effects in Fracture, ASTM STP 1171. American Society for Testing and Materials, pp. 21–40.

Hibbitt, Karlsson and Sorensen, Inc., 1997. ABAQUS Users Manual, Version 5.6-1, Providence, RI.

Hutchinson, J.W., 1968. Plastic stress and strain fields at a crack tip. Journal of the Mechanics and Physics of Solids 16, 337–347.

Jansson, S., 1986. Fully plastic plane stress solutions for biaxially loaded center-cracked plates. Journal of Applied Mechanics 53, 555–560.

Kachanov, L.M., 1974. Foundation of the Theory of Plasticity. Mir Publishers.

Kim, Y.-J., Lin, G., Cornec, A., Schwalbe, K.-H., 1996. Fully plastic crack-tip fields for plane strain shallow-cracked specimens under pure bending. International Journal of Fracture 78, 21–34.

Kumar, V., German, M.D., Shih, C.F., 1981. An Engineering Approach for Elastic-Plastic Fracture Analysis, EPRI Report NP-1931, Electric Power Research Institute.

Lee, J.D., Liebowitz, H., 1977. The nonlinear and biaxial effects on energy release rate, J-integral and stress intensity factor. Engineering Fracture Mechanics 9, 765–779.

Lee, H., Parks, D.M., 1993. Fully plastic analyses of plane strain single-edge-cracked specimens subject to combined tension and bending. International Journal of Fracture 63, 329–349.

Leevers, P.S., Radon, J.C., 1982. Inherent stress biaxiality in various fracture specimen geometries. International Journal of Fracture 19, 311–325.

Lei, Y., Neale, B.K., 1997. The fracture behaviour of a centre cracked tensile specimen. Fatigue and Fracture in Engineering Materials and Structures 20, 201–216.

McClintock, F.A., 1971. Plasticity aspects of fracture. In: Liebowitz, H. (Ed.), Fracture: An Advanced Treatise, vol. 3. Academic Press, New York, pp. 47–225.

Miller, A.G., 1988. Review of limit loads of structure containing defects. International Journal of Pressure Vessels and Piping 32, 197–327.

O'Dowd, N.P., Kolednik, O., Naumenko, V.P., 1999. Elastic-plastic analysis of biaxially loaded center-cracked plates. International Journal of Solids and Structures 36, 5639–5661.

O'Dowd, N.P., Shih, C.F., 1992. Family of crack-tip fields characterized by a triaxiality parameter — II. Fracture applications. Journal of the Mechanics and Physics of Solids 40, 939–963.

Prandtl, L., 1920. Ueber die Haerte plastischer Koerper. Goettinger Nacher., math.-phys. Kl, 74–85.

Quirk, A., Bevitt, E., 1991. Crack stability in center cracked plates subject to uniformly-distributed loadings. In: Kussmaul, K. (Ed.), Fracture Mechanics Verification by Large — Scale Testing. EGF/ESIS8 Mechanical Engineering Publications, London, pp. 87–103.

Quirk, A., Finnear, T.C., Fearnehough, G.D., Nichols, R.W., 1966. An experimental study of the failure strength of flawed steel plates. Nuclear Engineering Design 4, 39–53.

Shaw, D., Huang, Y.H., 1990. Buckling behavior of a central cracked thin plate under tension. Engineering Fracture Mechanics 35, 1019–1027.

Shih, C.F., deLorenzi, H.G., Andrews, W.R, 1979. Studies on crack initiation and stable crack growth. In: Landers, J.D., Begley, J.A., Clarke, G.A. (Eds.), Elastic-Plastic Fracture, ASTM STP 668. American Society for Testing and Materials, pp. 65–120.

Shih, C.F., German, M.D., 1981. Requirements for a one parameter characterization of crack tip fields by the HRR singularity. International Journal of Fracture 17, 27–43.

Shih, C.F., O'Dowd, N.P., Kirk, M.T., 1993. A framework for quantifying crack tip constraint. In: Constraint Effects in Fracture, ASTM STP 1171. American Society for Testing and Materials, pp. 2–20.

Wu, S.-X., Mai, Y.-W., Cotterell, B., 1990. Plastic η-factor (η_p) of fracture specimens with deep and shallow cracks. International Journal of Fracture 45, 1–18.

Yang, S., Chao, Y.J., Sutton, M.A., 1993. Higher order asymptotic crack tip fields in a power-law hardening material. Engineering Fracture Mechanics 45, 1–20.

Zhu, X.K., Chao, Y.J., 1999. Characterization of constraint of fully plastic crack-tip fields in non-hardening materials by the three-term solution. International Journal of Solids and Structures 36, 4497–4517.